

Toolpath Optimization for 3-Axis Milling of Thin-Wall Components



Niccolò Grossi, Lorenzo Morelli, and Antonio Scippa

Abstract Milling of thin-wall components often entails significant workpiece static deflections, which make manufacturers use conservative cutting parameters along the toolpath to meet the tolerance required. This paper presents a technique to define the 3-axis toolpath that maximizes cutting parameters, without compromising the accuracy of the component. This goal is achieved by coupling a FE model of the workpiece, updated to include material removal mechanism, to a mechanistic model of the cutting forces. The algorithm follows the milling cycle in the reverse order: starts from the finished part, computes the maximum allowable radial depth of cut, and adding material accordingly, generates the toolpath until the stock is build. The proposed technique has been experimentally validated through comparisons between milling tests and numerical results, both traditional and optimized toolpaths have been tested to assess accuracy, benefits and limitations of the method.

Keywords Toolpath · Milling · Thin-wall workpiece

1 Introduction

Milling is one of the most used technology in the mechanical industry thanks to its versatility and its accuracy. Unfortunately, the productivity of the process for flexible thin-wall parts, typical of the aerospace and energy sectors, is still limited by accuracy issues. Indeed, thin-wall components low rigidity entails errors on the surface caused

N. Grossi (✉) · L. Morelli · A. Scippa
Department of Industrial Engineering, University of Firenze, Via di Santa Marta 3, 50139 Firenze, Italy
e-mail: niccolo.grossi@unifi.it

L. Morelli
e-mail: lorenzo.morelli@unifi.it

A. Scippa
e-mail: antonio.scippa@unifi.it

by static deflection [1] and vibrations [2]. Focusing on dimensional tolerance (i.e., workpiece geometry errors), the key factor impacting on the accuracy is to be found in the workpiece static deflection caused by the cutting forces [3]. Since in-process methods to tackle this issue [4, 5] are expensive, time-consuming and difficult to be applied, virtual predictive techniques are the preference choice to build an integrated approach. These methods compute workpiece displacements based on cutting forces and workpiece compliance.

Different strategies have been proposed in literature to both handle the workpiece deflection and ensure the required tolerance: the ones focused on error compensation through a modified toolpath [6, 7] and the ones focused on the optimization of the process parameters (e.g., radial depth of cut) [8, 9].

Rao and Rao [6] developed an error compensation technique, which employs an analytical/numerical model to predict the part deflection that is adopted to compensate the toolpath. Ratchev et al. [7], instead, starts from an analytical force model integrated with a Finite Element (FE) model to estimate the workpiece deflection which is then used to offset the toolpath. The main disadvantage of compensation methods in 3-axis milling operations is that tool helix angle produces a variable surface error along the axial depth of cut direction [10], hence hardly to be compensated by a simple translation of the toolpath.

On the other hand, Wang et al. [8] and Koike et al. [9] proposed a parameter selection system to deal with workpiece deflections. Essentially, constant axial and radial depths of cut, chosen on maximum allowable deflection basis, are used to build blocks on the finished workpiece. Each one of these blocks represents a volume of the material that should be removed to obtain the final shape of the component. Sequence of cutting is defined starting from the finished part adding blocks according to the stiffness of the workpiece, till the whole stock is created. The main disadvantage of the method relies on the cutting parameters estimation that considers the predicted deflection error without compensating it. Moreover, since it is based on constant cutting parameters, axial and radial depths of cut are constrained by the most flexible point of the component, leading to low productivity, especially in the stiffest areas of the workpiece.

This paper presents a technique, for 3-axis milling operations, that generates an optimized toolpath ensuring the geometric tolerance on a thin-wall component. This strategy combines the benefits of the error compensation methods and parameters selection approaches and it considers the surface error variation along the axial depth of cut. Indeed, the method compensates the mean deflection which causes the geometric error and selects the process parameters to ensure that the deviation of the deflection, which cannot be compensated, satisfies the tolerance. In detail, the proposed method couples the actual workpiece stiffness during the material removal process, computed using a FE model based on 2D shell elements (Sect. 2.1), with the error prediction along the axial depth of cut obtained from the approach presented in [10] (Sect. 2.3). The algorithm starts from the final geometry, finding the most suitable point (i.e., end of the toolpath). Then it proceeds to the next points, adding material (according to the computed radial depth of cut), following the milling cycle in the reverse order, as in [8], but considering a variable radial depth of cut (Sect. 2.2).

Elaborating the order of the identified points and related radial depth of cut, optimized toolpath is generated (Sect. 2.4). The proposed technique has been experimentally validated on the 3-axis milling of a blade (NACA 0005 airfoil blade) (Sect. 3).

2 Proposed Approach

The proposed approach aims at computing the most suitable toolpath for 3-axis milling of thin-wall components to meet the target tolerance. The main features are: (i) best cutting sequence identification, (ii) radial depth of cut identification and (iii) compensation of the predicted surface error on the toolpath. To achieve the goals, the method, schematized in Fig. 1, is composed by several blocks summarized in four steps:

- Numerical model and workpiece stiffness prediction;
- Selection of layer and path (cutting sequence);
- Error along the axial depth of cut;

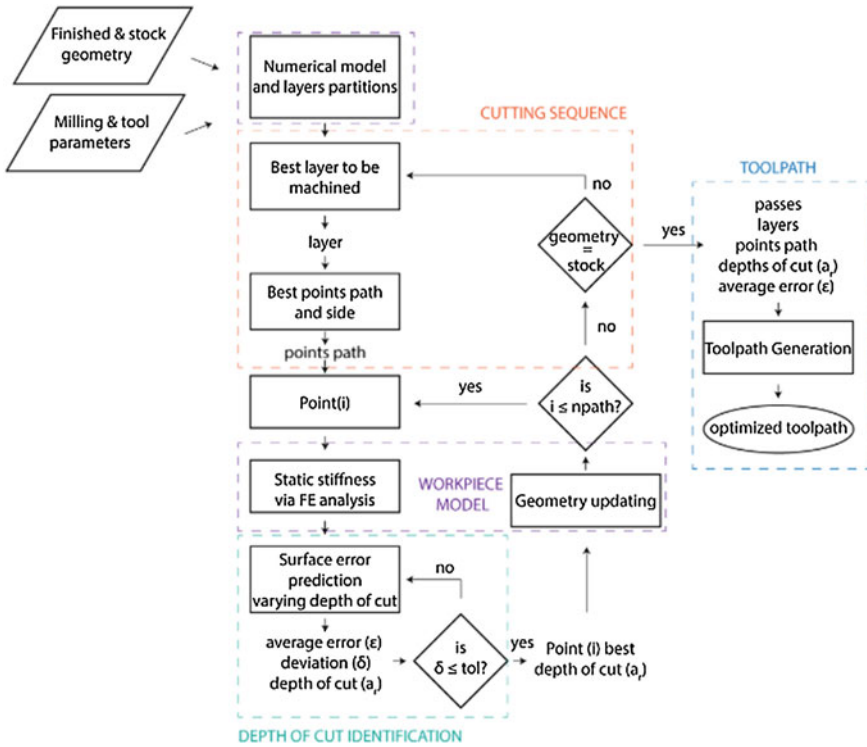


Fig. 1 Proposed approach scheme

- Toolpath generation.

Using the inputs (process parameters and tool data), the method reconstructs the best toolpath in a reverse order: starting from the finished part till the stock geometry is reached. First, the numerical model of the finished part is created by discretizing its geometry (i.e., FE model). Based on the axial depth of cut, the different layers to be machined are identified. For each layer, the machining allowance is computed as the difference on thickness between finished and stock geometry. The algorithm starts the loop by selecting the best layer among the ones available (i.e., the ones in which the machining allowance is not zero). From the selected layer on the finished part, the best path (cutting sequence) is then identified (i.e., the order of points). On each point in sequence, the radial depth of cut computation is performed. Radial depth of cut is selected as the highest value that allows to meet the target tolerance (input of the algorithm). Surface error is estimated by a dedicated algorithm that exploits cutting force prediction and static deformation of the workpiece in the cutting point, computed using FE analysis on the model. Once the radial depth of cut is identified, workpiece allowance and numerical model are updated. Radial depth of cut is computed for all the points along the path and the procedure is repeated till the stock geometry is reached. The sequence of layers, paths, radial depths of cut and surface errors are then used to build the toolpath, starting from the end of the computed cycle till the first step (i.e., finished part) is obtained. The algorithm, developed in Matlab, automatically arranges the FE analysis, performed using MSC Nastran. In the following sub-sections, the different blocks of the proposed technique are examined in depth.

2.1 Numerical Model and Workpiece Stiffness Prediction

Predicting workpiece stiffness is not a straightforward process, since the workpiece changes its geometry and hence its behavior during the machining cycle. Different strategies have been proposed in literature [5, 11, 12] most of them implies the use of Finite Element (FE) models, a convenient way to enable a virtual identification of workpiece behavior at different points and different machining steps. Ratchev et al. [11] developed an error compensation strategy for single pass peripheral milling based on FE method, while Budak [12] studied static displacements of cantilever plates milling with slender end-mills. Other authors simulate thin-wall components behavior for dynamics prediction purpose: Bolsunovskiy et al. [13] propose a method to compute the best spindle speeds to reduce the forced vibrations based on FE models of the thin-wall components, Tuysuz et al. [14] applied a reduced modeling technique on a full FE model of a thin-wall structure to predict chatter. All these works are based on 3D solid elements FE models, that for thin-wall components implies the use of small dimension elements, leading to high computational cost. This could be unacceptable when stiffness prediction should be performed several times to study workpiece deflection along the toolpath. In this work, the use of 2D shell elements

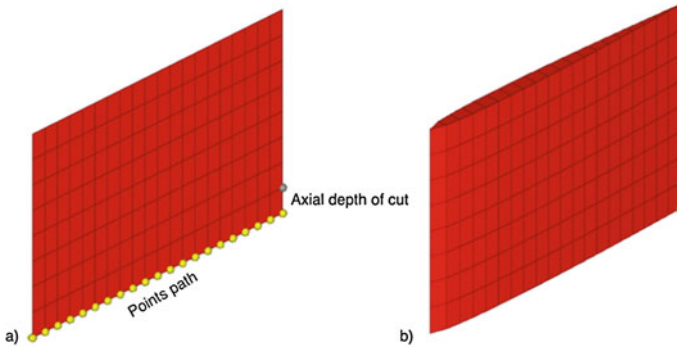


Fig. 2 Shell elements **a** 2D representation and characteristic nodes, **b** 3D representation

is proposed with a twofold advantage: (i) reducing computational efforts, (ii) easing both the automatic generation and updating of the thin-wall structure. Shell elements are suitable for thin-wall components and ensure the modeling of complex structure by using the mid-surface and variable thickness. In this work, mesh size on axial direction is selected equal to the axial depth of cut, while the mesh size on the other direction is selected to guarantee an accurate workpiece geometry discretization and behavior analysis.

The nodes on the mid line are the ones in which the optimal radial depth of cut is evaluated. On the axial direction two nodes are located limiting the axial depth of cut, as exemplified in Fig. 2. As previously mentioned, during the algorithm the mesh is automatically updated, allowing a fast generation of the toolpath. This is possible thanks to few operations: (i) node id are numbered in a specific order to be used by the algorithm to compile the analysis deck and launch the FE solver (e.g., Nastran), (ii) shell elements thickness will be based on the values given to the nodes (CQUAD4 card in Nastran [15]). This allows the procedure to automatically update the thickness of the nodes at each step by adding the computed radial depth of cut. In Fig. 3 an example of mesh updating procedure is presented. The algorithm starts with the mesh of the finished part (Fig. 3a), at the first point, radial depth of cut is computed, and thickness of the part is updated on the shell element (Fig. 3b), this procedure continues till all the nodes are analyzed and mesh updated (Fig. 3c). On the updated FE model of the workpiece at each step, static stiffness on the analyzed points is evaluated by performing a linear static analysis (SOL 101 in Nastran).

2.2 Selection of Layer and Points Path

The first step of the method is the identification of the cutting sequence. The idea is to build the toolpath, analyzing the cycle in the reverse order. The algorithm starts from the finished part and, at each step, finds the point where workpiece displacement

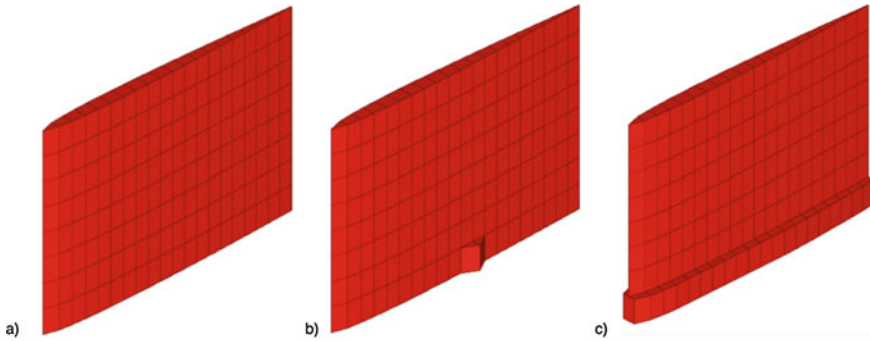


Fig. 3 Thickness updating **a** finished part, **b** first point updating, **c** full pass updating

due to the cutting forces is minimum. In that point, material is added (machining allowance is updated) according to the computed depth of cut, which is the maximum allowable value to meet the tolerance (Sect. 2.3). The algorithm stops when all the machining allowance is added to the final workpiece shape: i.e., stock geometry is achieved. Finally, the sequence is reversed to obtain the removal process. Cutting sequence in 3-axis milling is divided in: the layer to be machined (Z-axis) and the path on X–Y plane (points path), represented by the two nested loops of the algorithm (Fig. 1): (i) best layer selection; (ii) points path evaluation.

The first defines the axial position of the tool, while the second evaluates X–Y toolpath on the specific layer, analyzing all the points on the path. A new selection of the layer is repeated after that the points path evaluation procedure is completed, till the entire machining cycle is reconstructed. In general, layer selection should consider both machining constraints and flexibility of the components at several points, analyzing all the layers still to be machined (since the procedure is in the reverse order, a layer cannot be selected when it has already reached the stock dimension). This approach could not be trivial, since complex components and boundary conditions could benefit from a specific cutting sequence that enables the machining of the part in different zones in different conditions (i.e., time instant). In this paper, layer selection was implemented as simple as possible, considering only the flexibility of the component on one node at the same X–Y position and at the different heights (i.e., layers), performing a static analysis and choosing the stiffest layer. This approach is suitable for the investigated case of a cantilever plate and results in machining entirely each layer before going to the next from the top to the bottom. On the other hand, a more complex procedure that considers technological precedence and stiffness of the part in different points, not yet developed, is required in case of a more general application.

Once the layer is selected, points path within the layer is identified. For all the nodes of the layer, static stiffness is evaluated and the stiffest one is selected as the first node (i.e., the end of the path). In this work, the method is developed for open thin-wall components that needs to be machined on both sides. Therefore, the points path will pass through the same node twice. A procedure as the one proposed by

Wang et al. [8] would require the computation of the workpiece static stiffness in all the machinable points at every step of the machining cycle, leading to a very high computational cost. On the contrary, since a continuous machining cycle is preferable (as pointed out also in [8]), it is only required to define the first point and which side machines first. The side is selected based on the operation type (up or down milling) in order to reach the most flexible node (i.e., lowest static stiffness) on both sides when most of the material is still to be machined. Indeed, material on the part increases the local stiffness of the component, decreasing its deflection. Once the points path is defined, nodes in sequence will be analyzed to compute the maximum radial depth of cut allowable to meet the target tolerance, as explained in the next sub-section.

2.3 Error Along the Axial Depth of Cut

In peripheral milling, machined surface is generated at the instant in which tool passes over it (cutting edge perpendicular to the surface). Due to the helical nature of cutter, the axial location of surface generation points changes continuously with cutter rotation and the surface is created at different time instants. Since cutting forces are not constant over time, surface points along the tool axis are generated under the effect of different cutting forces. Therefore, even considering negligible the difference in terms of deflection between tool and workpiece along the tool axis, the surface error caused by the deflection of both the workpiece and the tool will change along the axial depth of cut and cannot be simply compensated by translating the original toolpath. In this work, surface error along the axial depth of cut is predicted by the formulations presented by Desai and Rao [10], extended to workpiece deflection, and a tailored compensation strategy was adopted. The surface error distribution depends on several factors, such as milling strategy (up or down milling), tool geometry (number of flutes and helix angle) and process parameters (axial and radial depth of cut). Starting from these input values, the three characteristic angles can be computed, α_{en} (radial engagement angle), α_{sw} (axial engagement angle) and φ_p (pitch angle) and used in the formulations to define the error shape. Error magnitude will depend on cutting forces and tool-workpiece stiffness. In this work, cutting force prediction is based on mechanistic force model adopting the following equations:

$$dF_t = K_t h db; \quad dF_r = K_r h db; \quad dF_a = K_a h db \quad (1)$$

where F_t , F_r , F_a are the tangential, radial and axial components of cutting force respectively, h is the uncut chip thickness and db is the chip width. Each of the force component is described by one coefficient related to material shearing and proportional to the chip thickness (K_t , K_r , K_a). As far as stiffness is concerned, tool stiffness will be measured and stored in the algorithm as input, while workpiece

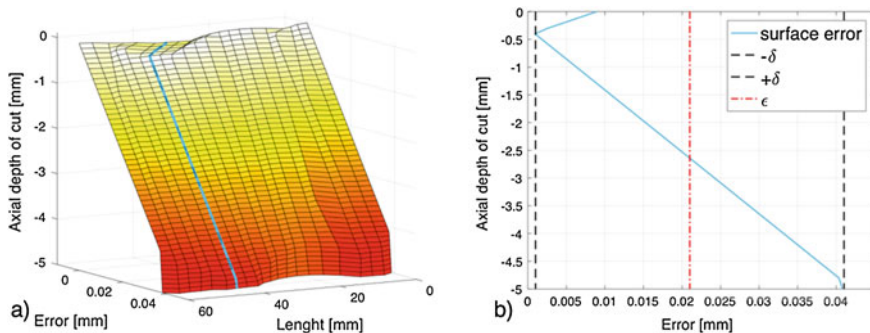


Fig. 4 Example of surface error **a** surface error prediction, **b** two error components

stiffness is computed using the FE model presented in the previous section. Using these data surface error distribution can be predicted and used to define toolpath.

In this method, two error components are distinguished: an average error (ϵ) and a deviation error (δ), as shown in the example in Fig. 4. The first (ϵ) will be compensated by offsetting the original toolpath, while the second (δ), that cannot be compensated in 3-axis, will be used in the algorithm to compute the most suitable radial depth of cut. Indeed, the value of deviation (δ) will change with the radial depth of cut and the maximum allowable value will be calculated in order to meet the target tolerance.

2.4 Toolpath Generation

The proposed algorithm (described in the previous sections), automatically selects: (i) the Z-axis position (i.e., layer), (ii) points path and (iii) radial depths of cut of the different passes to build the stock, starting from the finished part.

After collecting these data, toolpath is generated just reversing the passes and the points path and offsetting the stock geometry of Δ :

$$\Delta^i = \sum a_r^f + a_r^i + \epsilon \quad (2)$$

where a_r^f is the radial depth of cut of the following passes on the same node, a_r^i is the radial depth of cut computed for the specific pass and point, ϵ is the average error of the surface to be compensated. The sign of the offset depends on the side of the workpiece, sign of the error (ϵ) depends on the operations (down or up-milling).

3 Experimental Validation

The proposed approach has been experimentally validated on a 3-axis milling of a thin wall component, as case study. A NACA 0005 airfoil profile (60×40 mm), made of aluminum (6082-T4) has been machined on a DMU 75 machine tool, using a 12 mm diameter, four-fluted endmill (Garant 202552), starting from a stock with 6 mm of thickness and 60 mm overhang out of the clamp. To apply the proposed strategy, cutting force coefficients (Eq. 1) have been computed by using a mechanistic approach, based on the average cutting forces acquired on a specimen of the same material in slotting at 5 different feed per tooth (0.05–0.1–0.15–0.2–0.25 mm) and 2 depths of cut (0.5–1.0 mm) using a Kitsler 9257A table dynamometer (Fig. 5a). Experiments were replicated 3 times to improve the reliability and the resulting coefficients, including Confidential Interval CI (95%), are reported in Table 1. The toolpaths have been used to machine the test case on the CNC machine using the compensation of the cutter radius (G41), measured using an on-machine laser measuring system (BLUM Micro Compact NT 87) (Fig. 5d). Surfaces have been acquired using the on-machine probe (RENISHAW PowerProbe 60) (Fig. 5c). Tool static stiffness has been identified analyzing displacement/force Frequency Response Function, acquired using laser displacement sensor (Keyence LK-H085) and impact hammer (PCB 086C03) (Fig. 5b). The target tolerance of the part was set to ± 0.02 mm on a single side (i.e., ± 0.04 mm on the thickness of blade). These data along with tool and cutting parameters are summarized in Table 1.

Fig. 5 Machine set-up
a cutting force coefficient tests, **b** tool static stiffness measure, **c** machining error acquisition, **d** tool radius measure

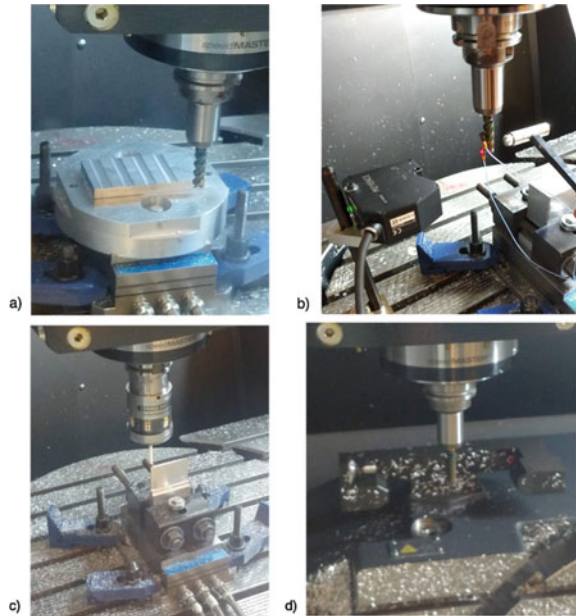


Table 1 Tool and cutting parameters

Tooling	Tool static stiffness		Cutting parameters				Cutting force coefficients				
	D (mm)	z	k_{rx} (N/mm)	k_{ry} (N/mm)	Tolerance (mm)	Strategy	ap (mm)	v_c (m/min)	f_z (mm)	K_t (N/mm ²) CI (95%)	K_r (N/mm ²) CI (95%)
45	12	4	4110	5710	±0.02	Down milling	5	200	0.1	752.9 ± 22.0	200.5 ± 12.5

3.1 Toolpath

Both a traditional toolpath and the optimized toolpath have been tested, using the same cutting parameters. Traditional toolpath consisted in leaving a small machining allowance (0.5 mm) over the finished part to be removed with the final passes. Finished and stock geometries were input to the developed algorithm and the procedure starts building the FE models (Fig. 6a–c). The FE model of the part is composed by 160 3×5 mm shell elements (CQUAD4 in Nastran), while the substrate (part not to be machined) was modelled via solid elements. The following mechanical characteristics were considered for the aluminum: elastic modulus 72.5 GPa, density 2680 kg/m³, Poisson’s ratio 0.34. Following the steps summarized in the previous sections the method reconstructed the optimized toolpath. Depths of cut and errors are computed by FE simulation on the nodes of the model, however generating the part program starting from FEM nodes by linear interpolation will imply a low resolution of the part or a very high computational cost (i.e., if the number of nodes is increased). Therefore, the part program is generated by linear interpolation of the toolpath on a new denser discretization of the geometry (50 times the number of

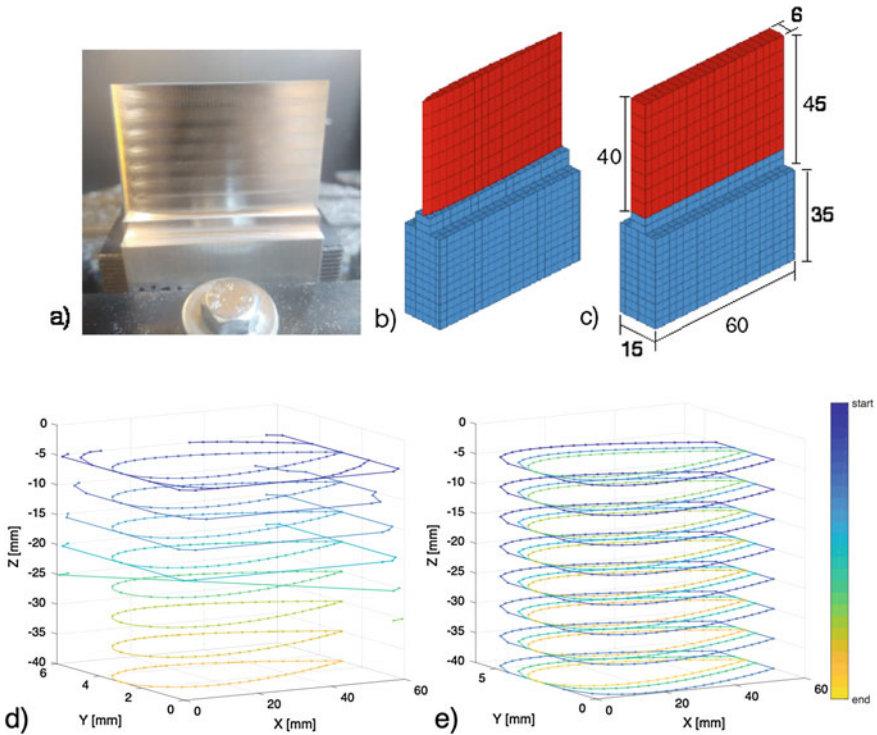


Fig. 6 Case study **a** physical, **b** finished FE model, **c** stock FE model with dimensions in mm, **d** optimized toolpath, **e** traditional toolpath

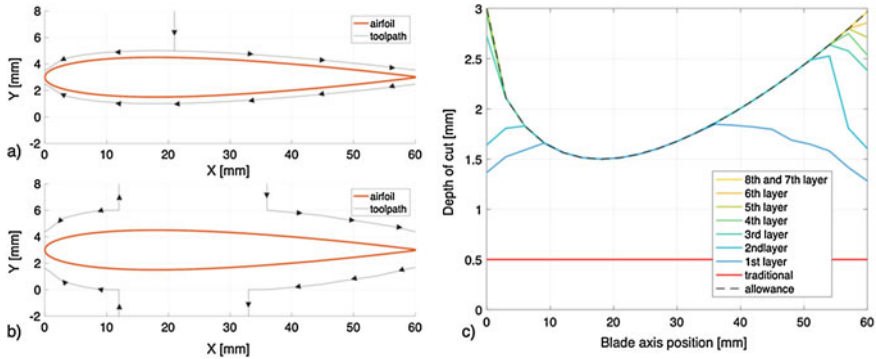


Fig. 7 a Example of traditional pass, b optimized pass, c depth of cut and machining allowance for traditional and optimized toolpath

points per line compared to the nodes of the FE model). Depths of cut and errors for this new discretization geometry are derived by linear interpolation of the values computed in the FE model nodes. By doing so, the computation cost is low (about 19 min in a laptop CPU 2.4 GHz Intel i5, RAM 4 GB for the whole optimization), while the resolution is high. Traditional and optimized toolpaths are presented in Fig. 6d, e.

The two toolpaths differ in both layers' selection and depths of cut. The proposed algorithm selects to machine each layer entirely before going on to the next and allows higher depths of cut on the final pass (around 1.5 mm against the 0.5 mm of the traditional toolpath). Moreover, as shown in Fig. 7 the selected depths of cut are not constant over the airfoil profile, indeed higher radial depths of cut are selected on the stiffer points (thicker part of the blade) and lower ones on the more flexible parts (trailing edge). Due to the evolution of the machining allowance (Fig. 7c), the proposed algorithm plans (multiple?) passes only on specific points (the more compliant), as shown in the example of Fig. 7a, while traditional approach consists in constant depth of cut passes, created by offsetting the airfoil geometry. In addition to this, as the tool goes down along the Z-axis, the number of passes at each layer decreases, since the stiffness of the component increases (Fig. 7c), proving that this strategy is in accordance with practical tips for thin-wall machining [16]. Thanks to the higher engagement conditions, the optimized toolpath machining cycle is faster than the traditional one: about 40 s against 90 s.

3.2 Machined Surface Results

To completely analyse the algorithm behaviour, machining surfaces have been acquired on each layer after being cut (interrupting the machining cycle before starting the next layer). For the sake of brevity, the machining errors on only one

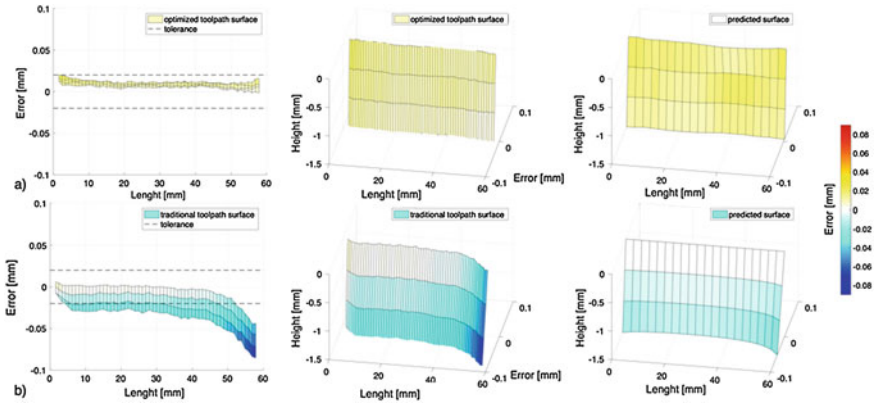


Fig. 8 Machining error on one side of the blade after machining the first layer **a** optimized toolpath, **b** traditional toolpath

side of the blade are presented (the results on the other side returned the same trend with opposite sign, i.e., the error on the thickness is double). Errors generated by the passes of the first layer (0/–5 mm) are presented in Fig. 8, for both traditional and optimized toolpath, including predicted values. For probe size reasons, only 1.5 mm could be measured. On the analyzed side of the blade, a negative error means a surface thicker than the nominal one, while positive means an overcutting of the surface.

As shown in Fig. 8a, optimized toolpath results in a low error surface (inside the tolerance range) almost constant all over the geometry, with good match between predicted and experimental errors. On the contrary, the first layer using the traditional toolpath (Fig. 8b) shows errors outside the tolerance range with higher value on the leading edge (i.e., the most flexible part). This trend was expected, since during down-milling, tool and workpiece static deflection causes an under-cut of the surfaces, not compensated by the traditional approach. Indeed, predicted surface is in line with the experimental results trend, even if an underestimation of the negative error on the leading edge is found. As soon as the most flexible layer is machined, the proposed approach manages to keep the error between the target tolerance (± 0.02 mm), while a different toolpath, that does not consider the flexibility of the system, generates higher errors (almost 0.1 mm).

In Fig. 9, the same analysis is reported on measured surfaces after machining the second layer (–5/–10 mm), measuring 0/–6.5 mm range. Optimized toolpath (Fig. 9a) after two layers keeps the same trend of the previous case: results are inside the tolerance with a peak at around 4 mm from the top. Even so, predicted values differ from experimental ones: errors are higher, and the peak is around 5 mm from the top. This difference is found also on the traditional toolpath. Thus, the traditional toolpath errors are still higher and outside the tolerance range but lower than the one in the previous case, even in the zone machined in the first layer (0–5 mm). This is caused by the second layer passes over the previous machined surface. Indeed, since the previous machined surface was thicker than the one desired, the second pass will

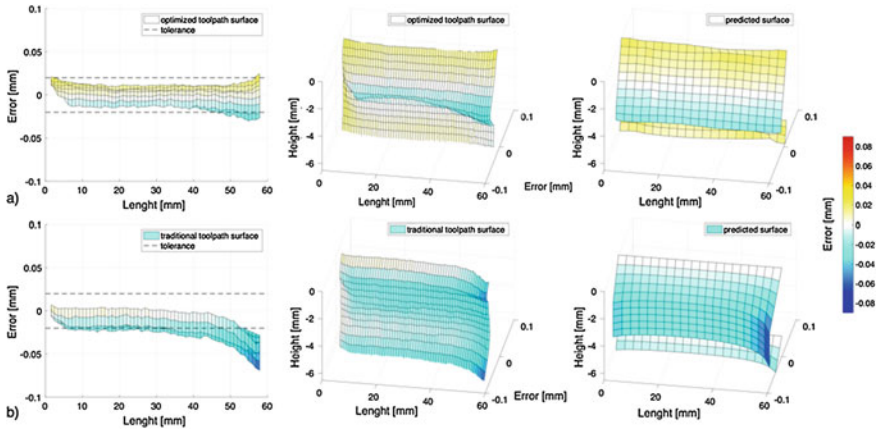


Fig. 9 Machining error on one side of the blade after machining the second layer **a** optimized toolpath, **b** traditional toolpath

also cut part of the previous surface. This effect is not considered by the algorithm, resulting in differences between predicted and actual surface errors. Nevertheless, after two layers the proposed algorithm can return a surface in tolerance, as desired, in contrast with the traditional toolpath that, even with this auto-leveling approach, fails to obtain a surface in tolerance. In fact, also the second layer presents a high compliance, resulting in a significant error on the surface.

This auto-leveling effect is even more advantageous in the machining of the whole case study, since the last passes on the stiffest part of the blade will affect the entire surface, reducing the actual error. This aspect is shown in Fig. 10, where the results

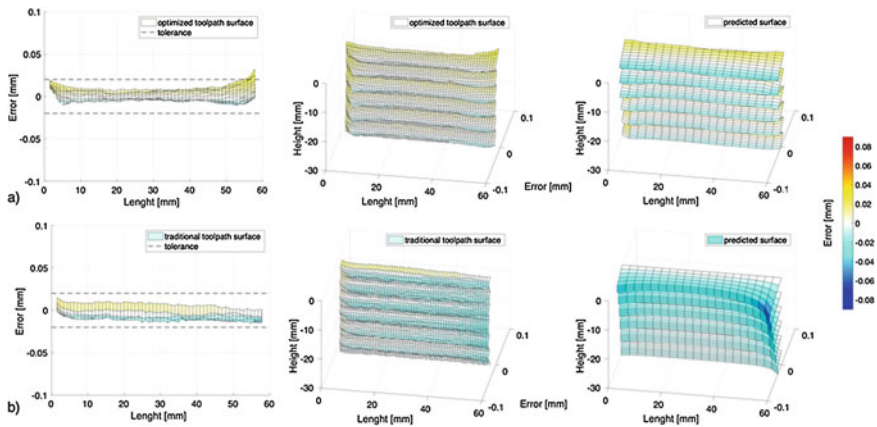


Fig. 10 Machining error on one side of the blade after the full machining cycle **a** optimized toolpath, **b** traditional toolpath

for the surface measured after the whole machining cycle (0/–40 mm) are presented (measures on 0/–30 mm range).

Figure 10 shows that, after the whole machining cycle is completed, both toolpaths produce surfaces inside the tolerance. Indeed, the machining errors of the traditional toolpath created by the passes on the first and the second layers have been drastically reduced by the passes on the following layers: the final passes on the last layer cut the oversized part of the blade in the upper zone, leveling the final surface. The effect is significant for multi passes 3-axis milling operations, especially in down-milling in which errors on the surface caused by deflection and cutting force lead to an under-cut of the surface (i.e., thicker part). On the contrary, single pass contouring operations and up-milling process should not be influenced by this effect. The proposed algorithm for error prediction (Sect. 2.3) does not include this effect, hence it overestimates the error for both toolpaths, however the method still provides an optimized toolpath that meets the target tolerance, reducing the number of passes and the cutting time.

4 Conclusions

In this paper, a technique to build the toolpath for 3-axis milling operations of thin-walled components is proposed. The method is the first step of the development of an integrated and automatic approach for toolpath generation, aiming to consider the flexibility of both the tool and the workpiece to select cutting parameters (i.e., engagement conditions), overcoming the limits of CAM software, that considers only the kinematic of the process. In this work, this procedure is developed for 3-axis milling: the algorithm generates the optimized toolpath, selecting the best cutting sequence (layers sequence and points path) to reduce the deflection of the component and computes the optimized radial depth of cut to keep the surface error in tolerance, given the other cutting parameters (e.g., axial depth of cut and feed). The method was experimentally validated and found to be accurate in predicting surface errors and computing the optimized toolpath in a single pass, reaching the target tolerance, while a traditional approach fails. On multi-passes, experimental results show that, in 3-axis down-milling, an auto-levelling effect was found. This effect is not included in the proposed approach and limits its application to single-pass contouring milling operations, where marks of the axial depth of cut are not acceptable, or multi-passes in up-milling process (where deflection causes an over-cut of the surface).

The presented technique lays the ground for the development of a more general approach, aiming at considering the flexibility of both the tool and the workpiece in the generation of the milling cycle. In addition to the radial depth of cut, the method could include the axial depth of cut and the feed to optimize the toolpath. Moreover, the method could be extended to simulate both more complex operations, such as 5-axis milling and additional effects, such as forced vibrations and unstable vibrations, since the FE model can be used to predict workpiece dynamics.

Acknowledgements The authors would like to thank Machine Tool Technology Research Foundation (MTTRF) and its supporters for the loaned machine tool (DMG MORI DMU 75 MonoBlock).

References

1. Sagherian R, Elbestawi MA (1990) A simulation system for improving machining accuracy in milling. *Comput Ind* 14(4):293–305
2. Budak E, Tunç LT, Alan S, Özgüven HN (2012) Prediction of workpiece dynamics and its effects on chatter stability in milling. *CIRP Ann* 61(1):339–342
3. Budak E, Altintas Y (1995) Modeling and avoidance of static form errors in peripheral milling of plates. *Int J Mach Tools Manuf* 35(3):459–476
4. Kolluru K, Axinte D (2013) Coupled interaction of dynamic responses of tool and workpiece in thin wall milling. *J Mater Process Technol* 213(9):1565–1574
5. Huang N, Yin C, Liang L, Hu J, Wu S (2018) Error compensation for machining of large thin-walled part with sculptured surface based on on-machine measurement. *Int J Adv Manuf Technol* 96(9):4345–4352
6. Rao VS, Rao PVM (2006) Tool deflection compensation in peripheral milling of curved geometries. *Int J Mach Tools Manuf* 46(15):2036–2043
7. Ratchev S, Liu S, Becker AA (2005) Error compensation strategy in milling flexible thin-wall parts. *J Mater Process Technol* 162–163:673–681
8. Wang J, Ibaraki S, Matsubara A (2017) A cutting sequence optimization algorithm to reduce the workpiece deformation in thin-wall machining. *Precis Eng* 50:506–514
9. Koike Y, Matsubara A, Yamaji I (2013) Design method of material removal process for minimizing workpiece displacement at cutting point. *CIRP Ann* 62(1):419–422
10. Desai KA, Rao PVM (2012) On cutter deflection surface errors in peripheral milling. *J Mater Process Technol* 212(11):2443–2454
11. Ratchev S, Liu S, Huang W, Becker AA (2006) An advanced FEA based force induced error compensation strategy in milling. *Int J Mach Tools Manuf* 46(5):542–551
12. Budak E (2006) Analytical models for high performance milling. Part I: cutting forces, structural deformations and tolerance integrity. *Int J Mach Tools Manuf* 46(12–13):1478–1488
13. Bolsunovskiy S, Vermel V, Gubanov G, Kacharava I, Kudryashov A (2013) Thin-walled part machining process parameters optimization based on finite-element modeling of workpiece vibrations. *Procedia CIRP* 8:276–280
14. Tuysuz O, Altintas Y (2017) Frequency domain updating of thin-walled workpiece dynamics using reduced order substructuring method in machining. *J Manuf Sci Eng* 139(7):71013–71016
15. Software Corporation MSC (2010) MD/MS Nastran 2010 quick reference guide
16. Altintas Y (2012) Manufacturing automation: metal cutting mechanics, machine tool vibrations, and CNC design